www.nature.com/aps

Acta Pharmacologica Sinica

ARTICLE

Increased S1P induces S1PR2 internalization to blunt the sensitivity of colorectal cancer to 5-fluorouracil via promoting intracellular uracil generation

Yu-hang Zhang[1], Shu-xiang Cui[2], Sheng-biao Wan[3], Shu-hua Wu[4] and Xian-jun Qu[1]

Sphingosine-1-phosphate (S1P), the backbone of most sphingolipids, activating S1P receptors (S1PRs) and the downstream G protein signaling has been implicated in chemoresistance. In this study we investigated the role of S1PR2 internalization in 5-fluorouracil (5-FU) resistance in human colorectal cancer (CRC). Clinical data of randomly selected 60 CRC specimens showed the correlation between S1PR2 internalization and increased intracellular uracil ($P < 0.001$). Then we explored the regulatory mechanisms in CRC model of villin-*S1PR2*$^{-/-}$ mice and CRC cell lines. We showed that co-administration of S1P promoted S1PR2 internalization from plasma membrane (PM) to endoplasmic reticulum (ER), thus blunted 5-FU efficacy against colorectal tumors in WT mice, compared to that in *S1PR2*$^{-/-}$ mice. In HCT116 and HT-29 cells, application of S1P (10 μM) empowered S1PR2 to internalize from PM to ER, thus inducing 5-FU resistance, whereas the specific S1PR2 inhibitor JTE-013 (10 μM) effectively inhibited S1P-induced S1PR2 internalization. Using Mag-Fluo-AM-labeling $[Ca^{2+}]_{ER}$ and LC-ESI-MS/MS, we revealed that internalized S1PR2 triggered elevating $[Ca^{2+}]_{ER}$ levels to activate PERK-eLF2α-ATF4 signaling in HCT116 cells. The activated ATF4 upregulated RNASET2-mediated uracil generation, which impaired exogenous 5-FU uptake to blunt 5-FU therapy. Overall, this study reveals a previously unrecognized mechanism of 5-FU resistance resulted from S1PR2 internalization-upregulated uracil generation in colorectal cancer, and provides the novel insight into the significance of S1PR2 localization in predicting the benefit of CRC patients from 5-FU-based chemotherapy.

Keywords: colorectal cancer; 5-FU resistance; sphingosine-1-phosphate (S1P); S1PR2 internalization; endoplasmic reticulum calcium ($[Ca^{2+}]_{ER}$); uracil generation; JTE-013

Acta Pharmacologica Sinica (2021) 42:460–469; https://doi.org/10.1038/s41401-020-0460-0

INTRODUCTION

5-Fluorouracil (5-FU) is a basic drug for the treatment of colorectal cancer (CRC), but it remains a major barrier for advances of favorable prognoses [1, 2]. Multiple mechanisms of innate and acquired 5-FU resistance have been suggested, such as high expression of thymidylate synthase and dihydropyridine dehydrogenase (DPD), aberrant epigenetic factors including microRNA, extrinsic factors, pH, hypoxia, paracrine interactions with stromal cells, and the modulation of autophagy [3–7]. A comprehensive understanding of the regulatory mechanism of 5-FU resistance is critical to determine the initial and subsequent regimens of specific therapeutics.

Sphingosine-1-phosphate (S1P) generated by sphingosine kinase (SphK) elicits a plethora of cellular responses, including the proliferation, survival, movement, angiogenesis, and multiple types of chemoresistance [8, 9]. These effects are mainly mediated through a family of five G protein coupled receptors (GPCRs), S1PR1-5, which are ubiquitously expressed and coupled to various G proteins that regulate numerous downstream signals [10, 11]. Among these receptors, S1PR1 and S1PR2 are widely expressed on most tissues. S1PR3 is highly expressed in the heart, lung, spleen, kidney, intestine, and diaphragm. S1PR4 is specifically expressed in lymphoid tissues and highly expressed on blood cells, whereas S1PR5 expression is restricted to the brain and skin and is highly expressed on natural killer cells [12]. These S1P receptors regulate diverse physiological processes in a highly specific manner, depending on their relative expression and that of G proteins.

Similar to the responses of other classes of receptors, prolonged stimulation of the natural ligand S1P often leads to the internalization of S1PRs into endosomes [13]. However, in contrast to classical GPCRs, the internalization of S1PR is often accompanied by persistent adenylyl cyclase (AC) inhibition at intracellular sites [14]. Upon internalization into human umbilical vein endothelial cells, S1PR1 was reported to localize to the Golgi/trans-Golgi network where it induces chemokinetic migration [15]. Apart from tissue-specific S1PR3-5, obscure functions of internalized S1PR2 await further exploration. In our previous study, we found that S1PR2 inhibitors potently reversed 5-FU resistance by prohibiting S1PR2 internalization, which downregulated DPD expression in CRC [16]. We also noticed that S1PR2 internalization

[1]Department of Pharmacology, School of Basic Medical Sciences, Capital Medical University, Beijing 100069, China; [2]Department of Toxicology and Sanitary Chemistry, School of Public Health, Capital Medical University, Beijing 100069, China; [3]Laboratory for Marine Drugs and Bioproducts of Qingdao National Laboratory for Marine Science and Technology, Key Laboratory of Marine Drugs, Ministry of Education, School of Medicine and Pharmacy, Ocean University of China, Qingdao 266100, China and [4]Department of Pathology, Hospital of Binzhou Medical University, Binzhou 264003, China
Correspondence: Xian-jun Qu (qxj@sdu.edu.cn)

Received: 5 March 2020 Accepted: 7 June 2020
Published online: 9 July 2020

is often accompanied by the increased generation of intracellular uracil in CRC cells. A recent study demonstrated that the upregulated generation of intracellular uracil prevented CRC cells from taking in FU as an exogenous uracil, blunting the CRC cell sensitivity to 5-FU therapy [17]. This finding inspired us to explore the underlying association between S1PR2 internalization and intracellular uracil generation.

In this study, we reveal that a previously unrecognized mechanism of 5-FU resistance is conferred by S1P-induced S1PR2 internalization, which is evident from the data of CRC patients, *S1PR2*$^{-/-}$ mice models and human CRC cell lines. We also shed light on the underlying mechanism by which S1PR2 is internalized by the endogenous S1P ligand, which can elevate $[Ca^{2+}]_{ER}$ levels and promote ER stress-mediated autophagy-related uracil yield by activating the ribonuclease RNASET2. It thus impairs CRC cell to uptake 5-FU as an exogenous uracil, resulting in attenuated 5-FU therapeutic effects. Overall, this study suggests that the localization of S1PR2 may be a robust predictive biomarker for the clinical response to 5-FU-based therapy regimens.

MATERIALS AND METHODS

CRC patients' specimens

Specimens were obtained from a total of 60 CRC patients randomly selected from 2009 to 2014, as approved by the Ethics Committee of Binzhou Hospital for use in this retrospective study (Ethical No. 2018-81772637-01). The patients had undergone the following therapies: either the 'de Gramont' regimen, delivered as a bolus infusion of 200 mg/m^2 leucovorin followed by a bolus of 400 mg/m^2 5-FU and 46 h of continuous 5-FU i.v. infusion (2400–3000 mg/m^2) or the 'Ardalan' regimen, consisting of 5-FU 2600 mg/m^2 administered weekly for 6 weeks followed by a 2-week rest period. The patient information and histopathological characteristics were obtained from the original pathology requisitions and physicians' notes, as shown in the chart information listed in Supplementary Table 1. Tumoral diagnoses, histological grades, and stages were independently reassessed under 100× magnification by two pathologists.

Villin-*S1PR2*$^{-/-}$ mice

All experiments related to animals were approved by the Animal Welfare Committee of Capital Medical University (Permit No. AEEI-2016-043). Mice were caged under controlled temperature, humidity, and light, and fed standard mouse chow. Villin-*S1PR2*$^{-/-}$ mice were generated by Cyagen Biosciences Inc. (Guangzhou, China) according to NC_000075.6 reference GRCm38.p6 C57BL/6J. To create *S1PR2*$^{-/-}$ by CRISPR/Cas-mediated genome engineering, we initially identified that the *s1pr2* gene in mice (Ensemble: ENSMUSG00000043895) was located in chromosome 9. Seven exons were identified, with an ATG start codon in exon 3 and a TGA stop codon in exon 7. The sequence from exon 3 to exon 7 was selected as the target site. Cas9 mRNA and gRNA generated by in vitro transcription were then injected into fertilized eggs of the *S1PR2*$^{-/-}$ mice (injected mRNA: S1PR2-gRNA3, VB161116-1055nbu). The founders were genotyped with PCR followed by DNA-sequencing analysis. The positive founders were bred to the next generation, which was genotyped by PCR and DNA-sequencing analysis. The PCR products were generated from PCR genotyping by using the primers listed in Supplementary Table 2. The amplicons were then purified and sent for DNA-sequencing analysis.

Stable transfection of shS1PR2 into cells

The HCT116 (ATCC® CCL-247™) and HT-29 (ATCC® HTB-38™) human CRC cell lines were purchased from the Cell Bank of China, as authorized by the ATCC, and seeded in six-well plates containing 2 mL of medium at a cell density of 40%–60% in each well. The medium was removed from the wells, and 2 mL of medium containing polybrene (final concentration of 5 μg/mL) was added to each well. The plate was gently swirled to mix the medium, which contained lentiviral particles that were removed from the wells. Fresh culture was substituted after 48 h, and then 500 μg/mL puromycin was added to the culture. After 7 to 10 days, the growth of the puromycin-resistant cells was observed, and the selected clones were grown in medium containing 200 μg/mL puromycin for 4 weeks. Puromycin-resistant clones, named shS1PR2 cells, were further propagated in medium containing 10% FBS in the absence of puromycin, and S1PR2 expression was determined by Western blotting. The transfection efficiency was affirmed by fluorescence microscopy. The scramble_shRNA of the lentivirus is LV-U6 > scramble-shRNA-PGK > EGFP/Puro. The control sequence was 5'-CCTAAGGTTAAGTCGCCCTCG-3', and the target sequence of S1PR2 was 5'-AGGAACAGCAAGTTCTACTCA-3' (founder #1).

Establishment of CRC in *S1PR2*$^{-/-}$ mice

CRC models were routinely established as previously described [18]. Briefly, mice were intraperitoneally injected with 10 mg/kg azoxymethane (AOM; Sigma-Aldrich). Then, for 1-week, all mice were repeatedly exposed to drinking water containing 1.0% dextran sodium sulfate (DSS, MP) and to three cycles of 2-week exposure to the treated water to establish CRC. All mice grew colorectal tumors with diameters from 3 to 10 mm. Their wild-type (WT) littermates were used for all experiments to ensure that the controls had the same genetic background.

Evaluation of the disease activity index (DAI)

Body weight, stool consistency, and rectal bleeding were recorded daily during the last 14 days of the experiment. The DAI was determined by summing the scores of body weight, stool consistency, and rectal bleeding. Each score was determined as follows: body weight loss (0, none; 1, 1%–5%; 2, 5%–10%; 3, 11%–15%; 4, 15%–30%; and 5, >30%); diarrhea (0, normal; 3, loose stools; and 6, watery diarrhea); and bleeding (0, normal; 4, slight bleeding; and 8, gross bleeding). The DAI score ranged from 0 to 19 (total score).

Immunoelectron microscopy

Colonic tissues were fixed with 4% glutaraldehyde, 2.5% paraformaldehyde in 0.1 M Sorensen's phosphate buffer (pH 7.4) for 1 h at room temperature. After washing the buffer from the samples, the tissues were added to 3% agarose and post fixed with 2.0% osmium tetroxide for 1 h at room temperature and then washed with buffer followed by distilled water. After rupturing the plasma membrane by Triton X-100, the tissues were incubated with S1PR2 antibody and colloid-labeled secondary antibodies. Then, after dehydration through a graded ethanol series, the tissues were infiltrated with and embedded in Embed 812 resin (Electron Microscopy Sciences). Thin sections were examined with a Hitachi 75000 electron microscope. The sections were analyzed under a Hitachi 75000 electron microscope.

Quantitative RT-PCR

Total RNA was isolated by using RNeasy Mini kit (74106, Qiagen). For cDNA synthesis, total RNA was transcribed by using Prime Script (DRR047A, TaKaRa, China). The levels of specific RNAs were measured by using an ABI 7900 real-time PCR machine and Fast SYBR Green PCR Master Mix according to the manufacturer's instructions. The relative number of target transcripts was normalized to the GAPDH expression in the same sample. The relative quantification of target gene expression was performed with the standard curve or comparative cycle threshold (CT) method. Fold change was calculated by using the CT method as follows: $\Delta\Delta CT = (CT_{\text{target gene}} - CT_{\text{housekeeping gene}})_{\text{treatment}} - (CT_{\text{target gene}} - CT_{\text{housekeeping gene}})_{\text{nontreatment}}$. The primer sequences are listed in Supplementary Table 2.

Immunohistochemistry (IHC) analysis
IHC analysis was routinely performed. Information on the primary antibodies is presented in Supplementary Table 3. The images obtained for the IHC analysis were scanned by a KF-PRO-OO5 scanner and a slide viewer.

Western blot analysis
Western blotting was routinely performed as previously described. All information on the primary antibodies is presented in Supplementary Table 3. The primary images (Supplementary Fig. 5) were cropped for presentation.

Immunofluorescence assay
HCT116 and HT-29 cells (2.5×10^4) were seeded onto glass coverslips in six-well plates. The cells were fixed in 4.5% paraformaldehyde for 15 min, washed in PBS, permeabilized with 1× Perm/Wash Buffer (BD Biosciences) for 10 min, washed in PBS, blocked to prevent nonspecific antibody reaction by incubating in a solution containing 5% BSA for 30 min and then with anti-calnexin or anti-S1PR2 antibodies. After incubation with secondary antibodies, the coverslips were mounted with VECTASHIELD® antifade mounting medium containing DAPI (Sigma-Aldrich). Confocal laser microscopy was performed with a Leica TCS SP5 AOBS apparatus using excitation spectral laser lines of 488 nm. Image acquisition and processing were conducted using Leica Confocal Software (Leica Microsystems).

Sphingolipid analyses
Lipids were extracted from the mouse colons, and phosphorylated and unphosphorylated spingoid bases were quantified by liquid chromatography and electrospray ionization-tandem mass spectrometry (LC-ESI-MS/MS) as described [19].

Small interfering RNAs (siRNAs)
siRNAs sequence for human GRP78 (5'-GCT CCT GAC TAT GCC AAA GC-3' and 5'-TCT TCA CCT CCA GGC TCA GT-3'), human PERK (5'-UAA AGG UGC UUU CAA UAA AUC CGG-3' and 5'-CCA GAG AAG UGG CAA GAA A-dTdT-3'), human ATF4 (5'-CUG CUU ACG UUG CCA UGA UTT AUC AUG GCA ACG UAA GCA GTT-3' and 5'-CCC UUC AGA UAA UGA UAG UTT ACU AUC AUU AUC UGA AGG GTT-3'), human Beclin1 (5'-GUG GAA UGG AAU GAG AUU ATT-3' and 5'-UAA UCU CAU UCC AUU CCA CTT-3'), human RNASET2 (5'-GCA AGA GAA AUU CAC AAA CUG CAG-3' and 5'-GCU GCA GUU UGU GAA UUU CUC UUG CUU-3') and control siRNA (5'-UUC UCC GAA CGU GUC ACG UdTdT-3' and 5'-ACG UGA CAC GUU CGG AGA AdTdT-3') were described previously. HCT116 cells were transfected both with siRNA and various expression vector constructs using Lipofectamine 2000.

Calcium labeling and confocal analysis
Specific fluorescent Mag-Fluo-AM probes (Genmed Scientifics Inc.) were used to label endoplasmic reticulum calcium ($[Ca^{2+}]_{ER}$). All labeling protocols were in strict accordance with the experimental instructions as described previously [20]. Then, 500 μL of cleaning solution was added to each dish to wash the cell debris. Then, 200 μL of dye solution (diluted 1:10) was added to each dish and incubated at 37 °C for 60 min. The dye solution was then removed, and 200 μL of cleaning solution and 2 μL of permeation solution were added and incubated at 37 °C for 4 min. Then, the dishes were washed with the cleaning solution and maintained in PBS for confocal microscopy assessment (Leica TCS SP5).

Metabolite extraction and analysis of uracil nucleosides by UHPLC-MS
After harvest, all the cells were rapidly frozen in liquid nitrogen to halt metabolism and stored at −80 °C until extraction. We extracted the metabolites of uracil according to reference [17]. Then, the nucleoside was analyzed by UHPLC-MS/MS (AB Sciex, QTRAP6500) equipped with a Waters ACQUITY UPLC HSS T3 column (100 × 2.1 mm, 1.8 μm). For the mobile phase, solution A was 10 mM ammonium acetate/formic acid, and solution B was methanol. For the standard solution preparation, stock solutions were individually prepared by dissolving or diluting each standard substance to a final concentration of 10 mM. A series of calibrated standard solutions were prepared by stepwise dilution of the standard solution. The concentrations of the RNA metabolites were calculated based on the respective calibration curves.

Statistical analysis
Statistical analysis was conducted with GraphPad Prism 8 software. After testing the data for normal distribution and variance homogeneity, continuous data were compared using a Mann–Whitney *U* test, multiple Student *t* tests or two-way ANOVAs. All *P* values are two-tailed, and *P* values < 0.05 were considered significant (*$P < 0.05$, **$P < 0.01$, and ***$P < 0.001$). The data are represented as the means ± SEM or the median with 10 and 90 percentiles. Chi-square tests of independence were used to measure the correlation between the expression levels of key molecules. DFS probabilities were estimated by the Kaplan–Meier method and were compared with the results of log-rank tests with SPSS 22.0. All statistical tests were two sided.

RESULTS

S1PR2 internalization is closely associated with intracellular uracil levels in human CRC specimens
To investigate the potential role of S1PR2 internalization in regulating 5-FU resistance, we randomly selected 30 patients' CRC specimens that had S1PR2 distributed in the plasma membrane (PM) and 30 patients' CRC specimens with internalized S1PR2 (Fig. 1a). The clinical information and histopathological characteristics are listed in Supplementary Table 1. As assayed by UHPLC-MRM-MS, the levels of S1P in the CRC tissues with internalized S1PR2 were much higher than they were in tissues with S1PR2 distribution in the PM ($P < 0.001$) (Fig. 1b). Notably, we also determined that the levels of intracellular uracil showed a twofold increase in the CRC tissues with internalized S1PR2 compared with those in the tissues with S1PR2 PM distribution (Fig. 1c).

Therefore, we analyzed 5-year disease-free survival (DFS) in the cohort of these 60 CRC patients. DFS was estimated using the Kaplan–Meier method, described as the median at specific time points with 95% confidence interval (CI), and the values were compared by log-rank test. The association of the baseline parameters with DFS was assessed by a multivariable Cox regression model, and the assumption of proportionality was tested by plotting log-minus-log survival curves and cumulative martingale plots. Of the 60 selected patients, all completed the study (none withdrew). Moreover, no significant differences were identified between the two groups of patients with internalized and PM S1PR2 in terms of their baseline characteristics (Supplementary Table 1). The results showed that patients with S1PR2 internalization (30 cases, 5-year OS rate = 0.32, 95% CI: 0.19–0.46) had worse outcomes than those with S1PR2 on the PM (30 cases, 5-year OS rate = 0.70, 95% CI: 0.57–0.80) after 5-FU-based therapy (Fig. 1d). These data indicated that S1PR2 internalization might be induced by increased S1P levels associated with higher uracil levels and worse prognosis for 5-FU therapy.

S1P promotes S1PR2 internalization to trigger 5-FU resistance in vivo
To confirm the roles of S1PR2 internalization in mediating 5-FU resistance, we analyzed the sensitivity of CRC to 5-FU in villin-*S1PR2*$^{-/-}$ mice and their WT littermates. Villin-*S1PR2*$^{-/-}$ mice specifically demonstrated lower S1PR2 expression in intestinal

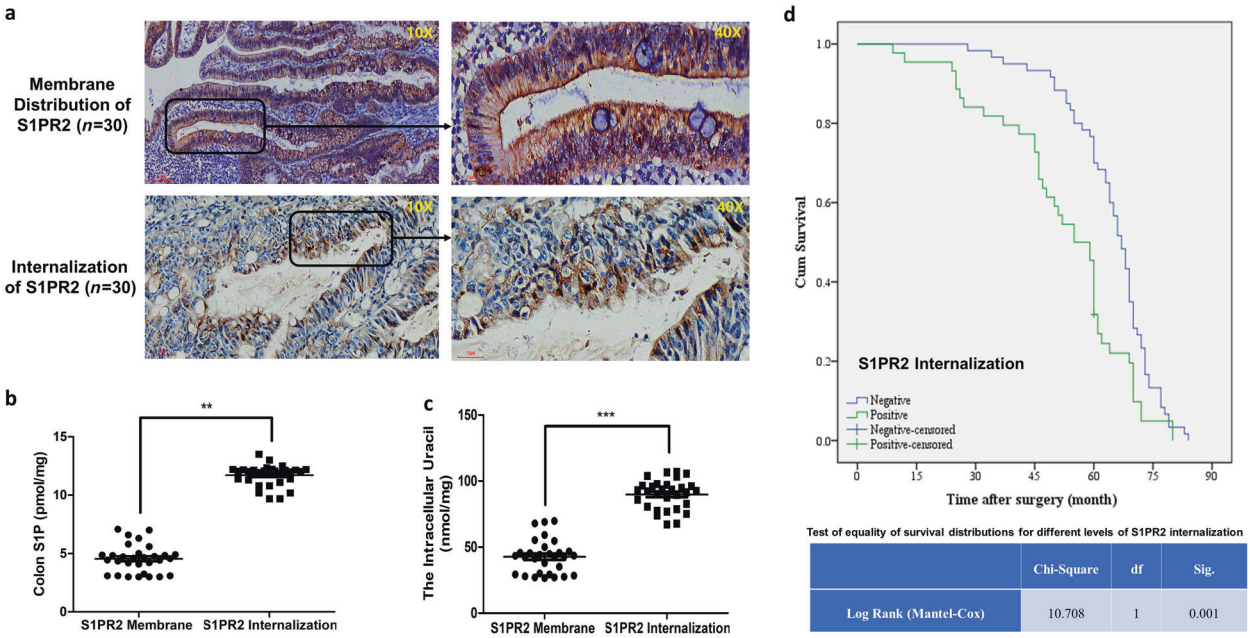

Test of equality of survival distributions for different levels of S1PR2 internalization

	Chi-Square	df	Sig.
Log Rank (Mantel-Cox)	10.708	1	0.001

Fig. 1 S1PR2 internalization is closely associated with intracellular uracil levels in human CRC specimens. a IHC assay showing CRC specimens with plasma membrane (PM) distribution of S1PR2 and CRC specimens with internalized S1PR2, $n = 30$ for each group (scale bar of left panel: 100 μm, scale bar of right panel: 30 μm). **b** The levels of S1P in colorectal cancer tissues obtained from the CRC specimens with PM distribution of S1PR2 and CRC specimens with internalized S1PR2. The levels of S1P were measured by LC-ESI-MS/MS assay, $n = 30$ for each group. **c** The levels of intracellular uracil in colorectal cancer tissues obtained from CRC specimens with PM distribution of S1PR2 and CRC specimens with internalized S1PR2. The levels of intracellular uracil were measured by LC-ESI-MS/MS assay, $n = 30$ for each group. **d** Kaplan–Meier curve analysis of the clinical outcomes of CRC patients with PM distribution of S1PR2 (30 cases, 5-year OS rate = 0.70, 95% CI: 0.57–0.80) and CRC specimens with internalized S1PR2 (30 cases, 5-year OS rate = 0.32, 95% CI: 0.19–0.46). Data in (**b**, **c**) are presented as the means ± SEM. $^{*}P < 0.05$, $^{**}P < 0.01$, and $^{***}P < 0.001$ (Student's t test).

epithelial cells (Supplementary Fig. 1a). All the mice were routinely exposed to AOM and DSS to induce CRC [21]. Then, 10 mg/kg 5-FU and 1 mg/kg S1P were intraperitoneally injected twice a week for five consecutive weeks. Compared with that in the WT littermates, the CRC in the villin-*S1PR2*$^{-/-}$ mice demonstrated higher sensitivity to 10 mg/kg 5-FU therapy (Fig. 2a, the top panel), showing the effective inhibition of both the number and size of colorectal tumors (Fig. 2a, the bottom panel). Moreover, S1P treatment blunted 5-FU treatment in the colorectal tumors of WT mice but not in the villin-*S1PR2*$^{-/-}$ mice, according to the tumor numbers and sizes in the 5-FU group and 5-FU plus S1P groups of the villin-*S1PR2*$^{-/-}$ and WT mice (Fig. 2a). As expected, the DAI scores also showed that increased S1P-induced lower survival after 5-FU treatment of colorectal tumors in the WT mice but not in the villin-*S1PR2*$^{-/-}$ mice, as determined by body weight, stool consistency, and rectal bleeding scores recorded daily (Supplementary Fig. 1b).

Then, we sought to determine the subcellular localization of S1PR2 in the WT mice that were treated with 5-FU and 5-FU plus S1P. Assayed by immunoelectron microscopy to track S1PR2 in colorectal epithelial cells, S1PR2 labeled with 20 nm colloid was mostly localized in the plasma membrane of the CRC cells in the control mice treated with saline; however, colloid-labeled S1PR2 was localized to the ER in the 5-FU plus S1P-treated mice. In contrast, the colloid-labeled S1PR2 in mice subjected to 5-FU monotherapy was not found to translocate from the plasma membrane (Fig. 2b). Then, S1PR2 internalization was validated by immunofluorescence analysis. The results showed the strong colocalization of S1PR2 with calnexin (atypical ER tracker) in the 5-FU plus S1P-treated mice but not in solvent-treated or 5-FU-treated mice (Fig. 2c). Finally, we performed UHPLC-MRM-MS to determine the levels of intracellular uracil in the colorectal tissues of the villin-*S1PR2*$^{-/-}$ mice and WT mice. Compared with the negligible increase in S1P-treated villin-*S1PR2*$^{-/-}$ mice, the level of intracellular uracil was drastically elevated in the S1P-treated WT mice (from 19.35 ± 4.10 pmol/mg to 42.20 ± 1.10 pmol/mg). In addition, 5-FU monotherapy negligibly affected the generation of intracellular uracil in both villin-*S1PR2*$^{-/-}$ mice and WT littermates (Fig. 2d). This result thus suggested that S1P upregulated the levels of intracellular uracil by inducing S1PR2 internalization.

S1P induces S1PR2 to internalize from the PM to the ER in human CRC cells

S1P/S1PR2-mediated 5-FU resistance was also analyzed in human CRC cell lines. S1PR2 shRNA was transfected into HCT116 and HT-29 cells to establish HCT116^{shS1PR2} and HT-29^{shS1PR2} cells (Supplementary Fig. 2a and b). Then, we treated these cells with 10 μM S1P and 5-FU in a dose gradient from 1.25 to 20 μM. The results showed that the shRNA of S1PR2 significantly sensitized both the HCT116 and HT-29 cells to 5-FU treatment. The IC_{50} value of 5-FU was reduced from 13.25 μM (HCT116^{vector} cells) to 4.75 μM (HCT116^{shS1PR2} cells) (Fig. 3a), and from 21.14 μM (HT-29^{vector} cells) to 4.89 μM (HT-29^{shS1PR2} cells) (Supplementary Fig. 2c). In contrast, the addition of 10 μM S1P triggered 5-FU resistance in both the HCT116^{vector} and HT-29^{vector} cells, whereas S1P negligibly affected the IC_{50} values of 5-FU in the HCT116^{shS1PR2} and HT-29^{shS1PR2} cells (Fig. 3a, Supplementary Fig. 2c).

Then, we performed an immunofluorescent assay to determine the route of internalized S1PR2 in the S1P-treated HCT116 cells. The results showed that 10 μM S1P but not 10 μM 5-FU drove S1PR2 internalization from the PM to the ER. However, 10 μM JTE-013, a specific inhibitor of S1PR2 with a K_i value of 56.60 ± 16.79 nM [22], effectively prohibited the S1PR2 internalization induced by S1P (Fig. 3b). Moreover, S1PR2 internalization induced by S1P and its inhibition by JTE-013 followed a dose-dependent correlation from 1.25 to 10 μM (Supplementary Fig. 3a, b). The

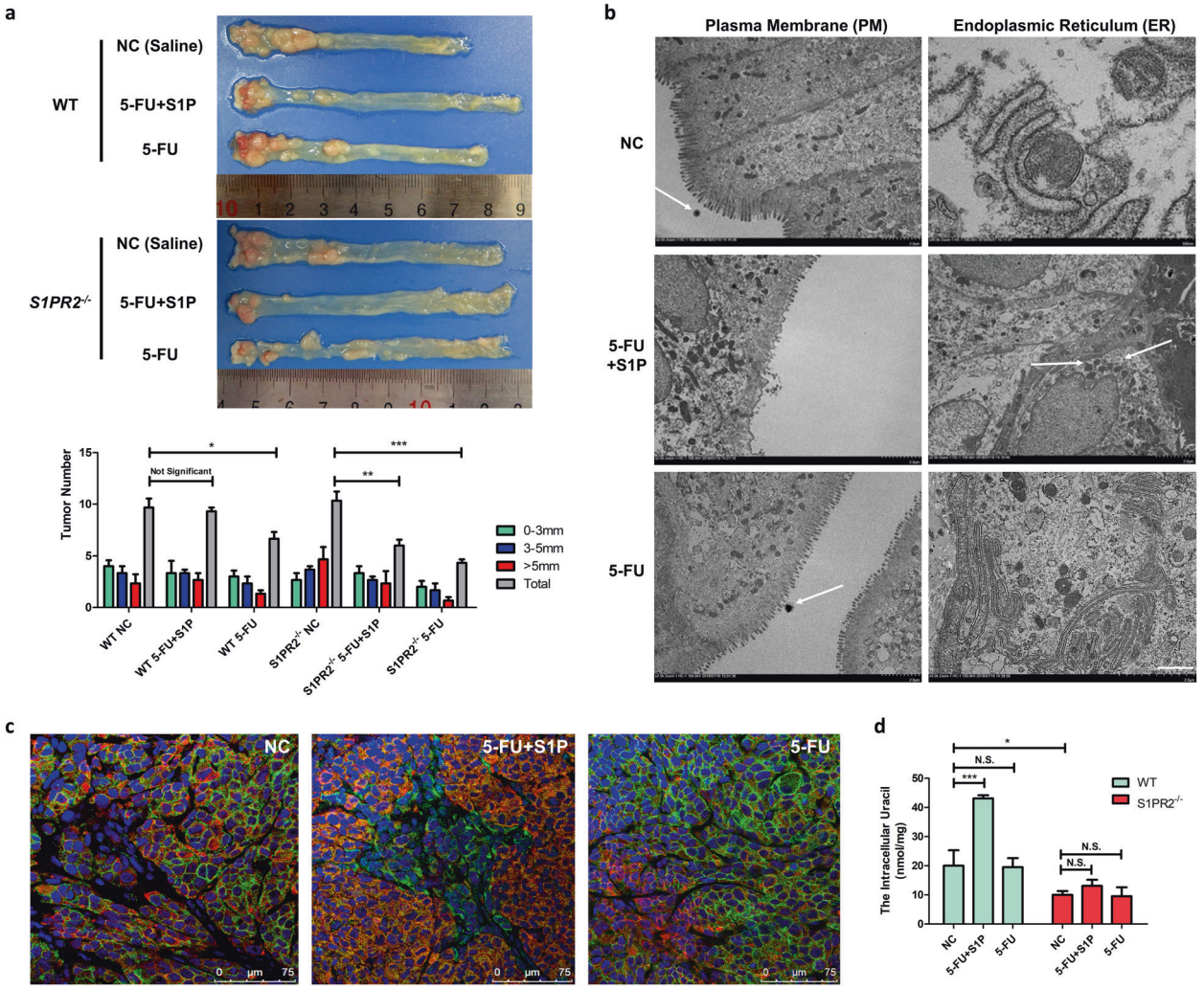

Fig. 2 S1P drives S1PR2 internalization to trigger 5-FU resistance in vivo. a The comparisons of colorectal tumor sensitivity to 5-FU and S1P treatment in the *S1PR2*$^{-/-}$ mice and their WT littermates. Therapeutic 5-FU of 10 mg/kg and S1P of 1 mg/kg were intraperitoneally injected twice a week for 5 weeks after the CRC model was established, $n = 6$ for each group. **b** S1PR2 in the PM was internalized to the ER in colorectal cancer cells of the WT mice undergoing 5-FU (10 mg/kg) plus S1P (1 mg/kg) therapy. However, 5-FU (10 mg/kg) monotherapy negligibly affected the localization of S1PR2. S1PR2 labeled with a 20 nm colloid was observed in the PM of cancer cells in the control 5-FU-treated WT mice. In contrast, colloid-labeled S1PR2 was clearly seen in the ER of cancer cells in the 5-FU plus S1P-treated mice (scale bar: 100 nm). **c** Determination of S1PR2 in the ER of colorectal cancer cells determined by immunofluorescence assay. S1PR2 (green) merged with the ER marker calnexin (red) in 5-FU plus S1P-treated mice, while S1PR2 (green) demonstrated PM distribution in the control and 5-FU-treated mice. S1PR2 internalization was observed only in CRC cells, not in hemocytes inside blood vessels (scale bar: 100 μm). **d** The levels of intracellular uracil in colorectal cancer tissues of *S1PR2*$^{-/-}$ mice and their WT littermates, which were treated with 10 mg/kg 5-FU combined with 1 mg/kg S1P. The levels of intracellular uracil were measured by LC-ESI-MS/MS assay, $n = 6$ for each group. Data in (**a**, **d**) are presented as the means ± SEM. $^{*}P < 0.05$, $^{**}P < 0.01$, and $^{***}P < 0.001$ (Student's *t* test).

ER translocation of S1PR2 was confirmed by Western blot analysis of the subcellular fractions of HCT116 and HT-29 cells obtained by ultracentrifugation. The quality of the 5%–20% (w/w) sucrose density gradient ultra-centrifuged fractions containing nuclei, mitochondria, and ER was analyzed by transmission electron microscopy (TEM) (Fig. 3c). Notably, 10 μM S1P induced S1PR2 internalization from the PM to the ER in both the HCT116 and HT-29 cells, but this subcellular translocation was prohibited by 10 μM JTE-013 (Fig. 3d, Supplementary Fig. 3c). Western blot analysis of subcellular organelles for the detection of laminB2 (nuclear tracker), AIF (mitochondrial tracker), and calnexin (ER tracker) also demonstrated the high purity of the subcellular fractions (Fig. 3d, Supplementary Fig. 3c). Next, the co-IP assay showed that S1PR2 coimmunoprecipitated from S1P-cultured HCT116 cells with calnexin antibody-coated immunomagnetic beads and vice versa (Fig. 3e, f). Blocking S1PR2 with 10 μM JTE-013 did not affect S1PR2 internalization to the ER in the S1P-treated HCT116 cells (Fig. 3e, f). Finally, we determined the levels of intracellular uracil in the HCT116 cells treated with 5-FU, S1P, or JTE-013. The intracellular uracil was drastically increased by 10 μM S1P treatment, from 6.31 ± 0.34 pmol/mg to 12.51 ± 3.10 pmol/mg. JTE-013 (10 μM) significantly decreased the S1P-upregulated intracellular uracil level to 8.42 ± 0.16 pmol/mg. These results suggest that S1P induces S1PR2 internalization to the ER, where it upregulates the generation of intracellular uracil.

S1P-induced S1PR2 internalization triggers $[Ca^{2+}]_{ER}$ perturbation to activate PERK-eIF2α-ATF4 signaling

It has been proposed that S1P mobilizes calcium in the endoplasmic reticulum (ER) independently of inositol trisphosphate ($InsP_3$) and its receptor ($InsP_3R$) [23, 24]. However, the targets (S1P receptors) of S1P on the ER have not yet been validated. Since we have found

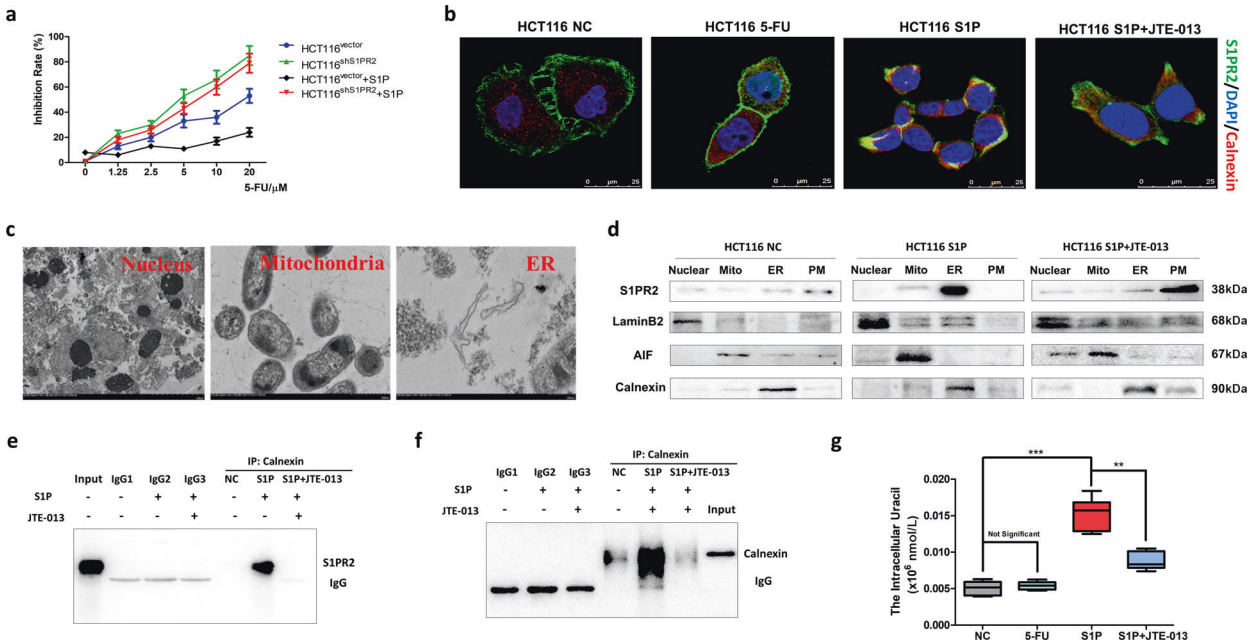

Fig. 3 S1P induces S1PR2 internalization from the PM to the ER in human CRC cells. a Inhibition rates of 5-FU were determined by MTT assay of the HCT116^{shS1PR2} and HCT116^{vector} cells treated with 10 μM S1P. The dose gradient of the 5-FU treatment ranged from 0 to 20 μM. Inhibition rate $= 1 - (OD_{Drug} - OD_{Blank})/(OD_{Control} - OD_{Blank})$, $n = 3$. **b** Immunofluorescence assay determined S1PR2 internalization in the HCT116 cells. S1PR2 maintained expression on the PM of the HCT116 cells treated with PBS or 10 μM 5-FU, while S1PR2 was internalized to the ER in the HCT116 cells exposed to 10 μM S1P. However, S1P-induced S1PR2 internalization was inhibited by 10 μM JTE-013 (scale bar: 25 μm). **c** Transmission electron microscopy was used to analyze the quality of the subcellular components separated by 5%–20% (w/w) sucrose density gradient ultracentrifugation into nuclear, mitochondrial and ER fractions of the HCT116 cells (scale bar: 100 nm). **d** Western blot analysis showed the levels of S1PR2, laminB2 (nuclear tracker), AIF (mitochondria tracker), and calnexin (ER tracker) in the nucleus, mitochondria (mito), ER and PM fractions, which were isolated from the HCT116 cells undergoing S1P and S1P plus JTE-013 treatments. **e**, **f** Co-IP assay indicated binding of S1PR2 and calnexin. S1PR2 was immunoprecipitated by magnetic beads with calnexin from the HCT116 cells exposed to 10 μM S1P or JTE-013 for 24 h. A substantial amount of S1PR2 was pulled down from cells treated with 5-FU, whereas no S1PR2 was pulled down when JTE-013 was added (**e**). Reciprocally, calnexin was also coimmunoprecipitated with S1PR2 upon the addition of 10 μM S1P, but immunoprecipitation failed when the cells were concurrently exposed to 10 μM JTE-013 for 24 h (**f**). **g** The concentration of intracellular uracil was measured by LC-ESI-MS/MS assay of the HCT116 cells, which were treated with 10 μM 5-FU, 10 μM S1P or 5-FU plus S1P for 24 h. Data are presented as the means ± SEM. $^*P < 0.05$, $^{**}P < 0.01$ and, $^{***}P < 0.001$ (Student's t test).

that S1PR2 is internalized to the ER to upregulate the generation of intracellular uracil, we sought to determine whether internalized S1PR2 mediates ER calcium ($[Ca^{2+}]_{ER}$) levels to promote uracil yield. To test our hypothesis, we used a fluorescent Mag-Fluo-AM probe to measure the changes in $[Ca^{2+}]_{ER}$ levels in the HCT116^{vector} and HCT116^{shS1PR2} cells which were under continuous 10 μM S1P exposure. As shown in Fig. 4a (i), the S1P-treated HCT116^{vector} cells showed a sharp increase in $[Ca^{2+}]_{ER}$ at 430 s, which reached a plateau between 1180 and 2000 s. In contrast, the $[Ca^{2+}]_{ER}$ levels in the HCT116^{shS1PR2} cells showed as low increase within 2000 s of S1P treatment. The peak concentration of $[Ca^{2+}]_{ER}$ in the HCT116^{shS1PR2} cells was only 17% that of the HCT116^{vector} cells (Fig. 4a, iii). The increased $[Ca^{2+}]_{ER}$ level was profoundly inhibited by JTE-013 in the HCT116^{vector} cells, but not in the HCT116^{shS1PR2} cells (Fig. 4a, ii and iv). Moreover, these results were consistent with the concentrations of $[Ca^{2+}]_{ER}$, as measured by a fluorescent microplate, in the HCT116^{vector} cells and HCT116^{shS1PR2} cells that were exposed to S1P or JTE-013 (Supplementary Fig. 4a). Overall, the level of Mag-Fluo-AM-probe $[Ca^{2+}]_{ER}$ in the HCT116^{vector} cells was increased with S1P addition but decreased with the inhibition of S1PR2.

Since the sensor of ER stress, GRP78, functions as a Ca^{2+}-binding protein in the ER [25], we speculated that perturbation of the $[Ca^{2+}]_{ER}$ can cause ER stress. TEM analysis of S1P-treated HCT116 cells showed typical ER stress, as characterized by the expansion of the ER lumen with double-membrane structures (Supplementary Fig. 4b, ii). However, JTE-013 reversed S1P-induced ER stress and maintained the integrity of the ER lumen (Supplementary Fig. 4b, iii). Then, we demonstrated that the increased $[Ca^{2+}]_{ER}$ level influenced ER stress through the GRP78-PERK-eIF2*α*-ATF4 pathway. This conclusion was supported by the Western and quantitative RT-PCR data obtained from the HCT116^{vector} and HCT116^{shS1PR2} cells that were treated with 10 μM S1P and 10 μM JTE-013. The expression of GRP78, P-eIF2*α* and, ATF4 was upregulated by S1P but downregulated by shS1PR2 or JTE-013 (Fig. 4b, Supplementary Fig. 4c). Moreover, we also confirmed the roles of GRP78 and PERK in mediating the S1P-activated eIF2*α*-ATF4 axis in the HCT116^{GRP78siRNA} and HCT116^{PERKsiRNA} cells, revealing that inactivating GRP78 or PERK suppressed the expression of P-eIF2*α* and ATF4 (Fig. 4c). In addition, knocking down GRP78 or PERK effectively sensitized the HCT116^{vector} cells, but not the HCT116^{shS1PR2} cells to 5-FU treatment. The IC_{50} values of 5-FU were significantly reduced from 13.24 to 3.12 μM and 7.40 μM by blocking GRP78 and PERK, respectively, in the HCT116^{vector} cells (Fig. 4d). In addition, neither IRE1*α* nor ATF6 closely correlated with S1PR2 internalization, and S1PR2 negligibly affected the transcription of *xbp1s* and *atf6(n)*. However, *grp78*, *atf4,* and *chop* were all transcriptionally upregulated by 10 μM S1P added to the HCT116^{vector} cells but were not affected in the HCT116^{shS1PR2} cells (Supplementary Fig. 4c). Overall, these results suggested that S1P induced S1PR2 internalization to activate the GRP78-PERK-eIF2*α*-ATF4 pathway in the ER.

Activated ATF4 upregulates RNASET2 to promote uracil generation, leading to 5-FU resistance of colorectal tumors

It is well known that ER stress-induced autophagy can trigger drug resistance [26–28]. Since internalized S1PR2 was found to activate ATF4 in the ER, we also investigated whether S1PR2 was involved in

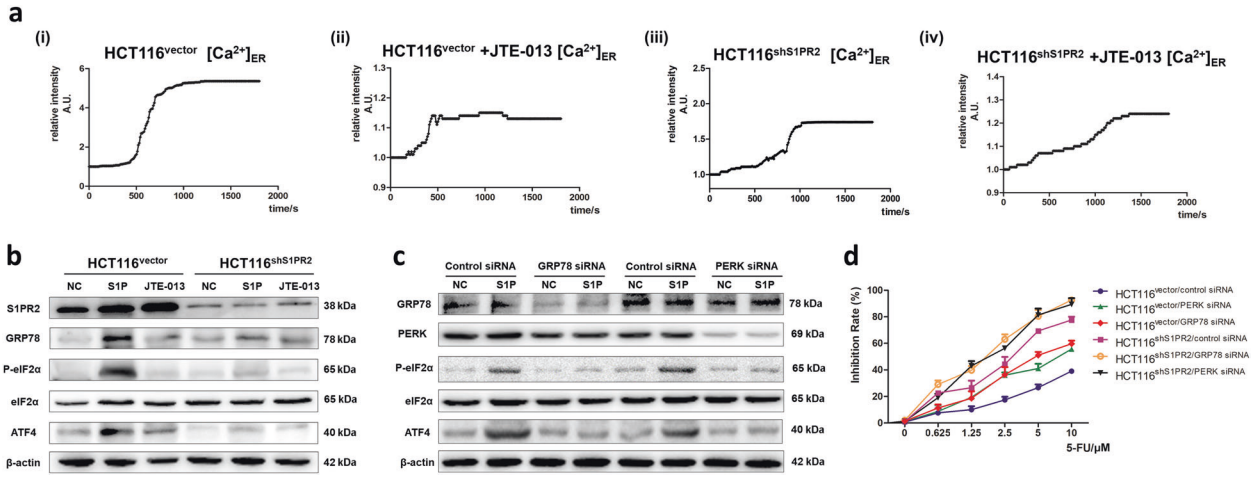

Fig. 4 S1P-induced S1PR2 internalization triggers $[Ca^{2+}]_{ER}$ perturbation to activate PERK-eIF2α-ATF4 signaling. a Mag-Fluo-AM probe was used to analyze the $[Ca^{2+}]_{ER}$ level in the $HCT116^{vector}$ (i) and $HCT116^{shS1PR2}$ cells (iii) and the respective JTE-013 (10 μM) treatment groups (ii and iv) undergoing S1P (10 μM) challenge for 30 min. The observation of dynamic $[Ca^{2+}]_{ER}$ levels within 30 min was photographed by confocal microscopy scanning every 10 s. **b** Western blot analysis showing the levels of GRP78-eIF2α-ATF4 in the human $HCT116^{vector}$ and $HCT116^{shS1PR2}$ cells treated with S1P (10 μM) and JTE-013 (10 μM). **c** Western blot analysis showing the levels of GRP78-eIF2α-ATF4 in the human $HCT116^{GRP78siRNA}$ and $HCT116^{PERKsiRNA}$ cells treated with 10 μM S1P for 24 h. **d** In the $HCT116^{vector}$ and $HCT116^{shS1PR2}$ cells, PKD1 and S1PR2 were knocked down by their respective siRNAs. The inhibition rates of 5-FU (24 h) were determined by MTT assay. The dose gradient of 5-FU treatment ranged from 0 to 10 μM. Inhibition rate $= 1 - (OD_{Drug} - OD_{Blank})/(OD_{Control} - OD_{Blank})$, $n = 3$.

modulating ATF4-associated autophagy signaling. It was reported that the transcription factor ATF4 can bind with the promoters of several gene markers of autophagy [29]. We thus performed a ChIP assay to analyze the transcriptional levels of the promoter regions of these autophagy genes in response to 10 μM S1P exposure. When $HCT116^{vector}$ and $HCT116^{shS1PR2}$ cells were exposed to S1P, strong binding of ATF4 to *Beclin1* was observed in the $HCT116^{vector}$ cells but not in the $HCT116^{shS1PR2}$ cells, and the binding of ATF4 to *Beclin1* in the $HCT116^{vector}$ cells could be blocked by JTE-013. In contrast, ATF4 weakly bound to *Atg7*, *Atg3*, and *Atg5* (Fig. 5a). Moreover, the activation of autophagy mediated by S1PR2 was evidenced by the Beclin1, LC3B, and p62 markers in the $HCT116^{shS1PR2}$ cells, $HCT116^{vector}$ cells and $HCT116^{S1PR2}$ cells (Fig. 5b). Importantly, the TEM analysis showed that the typical autophagic cargos and autophagosomes in the HCT116 cells exposed to 10 μM S1P exposure compared with the normal morphosis of intracellular lysosomes in naive HCT116 cells (Fig. 5c). In contrast, when ATF4, Beclin1, and RNASET2 were knocked down in the HCT116 cells, the IC_{50} values of 5-FU were substantially reduced, from 76.31 to 12.58, 10.48, and 7.85 μM, respectively (Fig. 5d).

RNASET2, the critical ribonuclease of the T2 family crucial for ribosomal RNA degradation in autophagolysosomes [30, 31], was upregulated by S1P but suppressed by JTE-013 in the HCT116 cells (Fig. 5b). It was reported that RNASET2-mediated autophagy-related uracil generation by degrading self-RNA into 3′UMP, 3′CMP, uridine and, cytidine. As uracil analogs, these RNA metabolites interfered with the uptake of exogenous 5-FU, leading to decreased 5-FU efficacy [17]. We performed a UHPLC-MRM-MS assay to analyze the contents of these uracil-related nucleosides and nucleobases in $HCT116^{vector}$ and $HCT116^{shS1PR2}$ cells. Strikingly, 3′UMP was increased in the $HCT116^{vector}$ cells for as long as 6 h, after which it gradually decreased. The uridine content was increased in the $HCT116^{vector}$ cells in a time-dependent manner, while depletion of S1PR2 prevented the increase in 3′UMP and uridine. In contrast, increases in 3′CMP and cytidine were not observed in the $HCT116^{vector}$ or $HCT116^{shS1PR2}$ cells (Fig. 5e, f). Ultimately, the levels of intracellular uracil were determined by UHPLC-MRM-MS assay, which showed a time-dependent increase in the $HCT116^{vector}$ cells but not in the $HCT116^{shS1PR2}$ cells (Fig. 5g, left panel). In addition, a time-dependent decrease in the 5-FU concentration was also detected in the $HCT116^{shS1PR2}$ cell culture but not in $HCT116^{vector}$ cell culture within 24 h of exposure to 10 μM S1P (Fig. 5g, right panel). Altogether, these results suggested that S1P-induced S1PR2 internalization upregulates the generation of intracellular uracil to block exogenous 5-FU uptake by activating RNASET2-mediated 3′ UMP-uridine-uracil metabolism (Fig. 5h).

DISCUSSION

Aberrant sphingolipid metabolism has been implicated in chemoresistance [32], but we did not concretely know the underlying mechanisms. Herein, we provide novel insights into the mechanism of 5-FU resistance as observed by S1P-induced S1PR2 internalization. The following major discoveries were made: (1) Increased S1P drives S1PR2 internalization from the plasma membrane to the endoplasmic reticulum; (2) internalized S1PR2 increases the levels of $[Ca^{2+}]_{ER}$ to activate PERK-eIF2α-ATF4 signaling; and (3) activated ATF4 upregulates RNASET2-mediated autophagy-related uracil generation, which impairs exogenous 5-FU uptake to blunt 5-FU therapy. In essence, this study suggests S1PR2 as the crucial upstream regulator of tumoral uracil generation and indicates that combination therapy with S1PR2-related inhibitors such as JTE-013 might be a potential strategy to overcome 5-FU resistance in CRC patients.

It was reported that conversion to S1P can lower sphingosine levels and thus disinhibit store-operated calcium release-activated calcium current (I_{CRAC}), which thereby increased calcium influx [33]. Although several current reports support the idea that SphK is involved in calcium mobilization [34, 35], the supposition is still subjective because intracellular targets in the ER that are critical for the effects of S1P have not been identified. Herein, we show that S1P-induced S1PR2 internalization to the ER. This finding explicitly indicates that S1PR2 might be the ER-localized S1PR that mediates $[Ca^{2+}]_{ER}$, as evidenced in the human CRC specimens, animal models, and cancer cell lines. In addition, GRP78 functions as the Ca^{2+}-binding protein in the ER [25], and our results showed that GRP78 was upregulated to activate the PERK-eIF2α-ATF4 pathway, which validates the effects of S1PR2 internalization in the ER.

Ca^{2+} and cAMP are two fundamental second messengers that govern a vast array of cellular functions but also regulate each other on multiple levels [36]. Changes in cytosolic Ca^{2+} levels are known to either enhance or depress cAMP production through

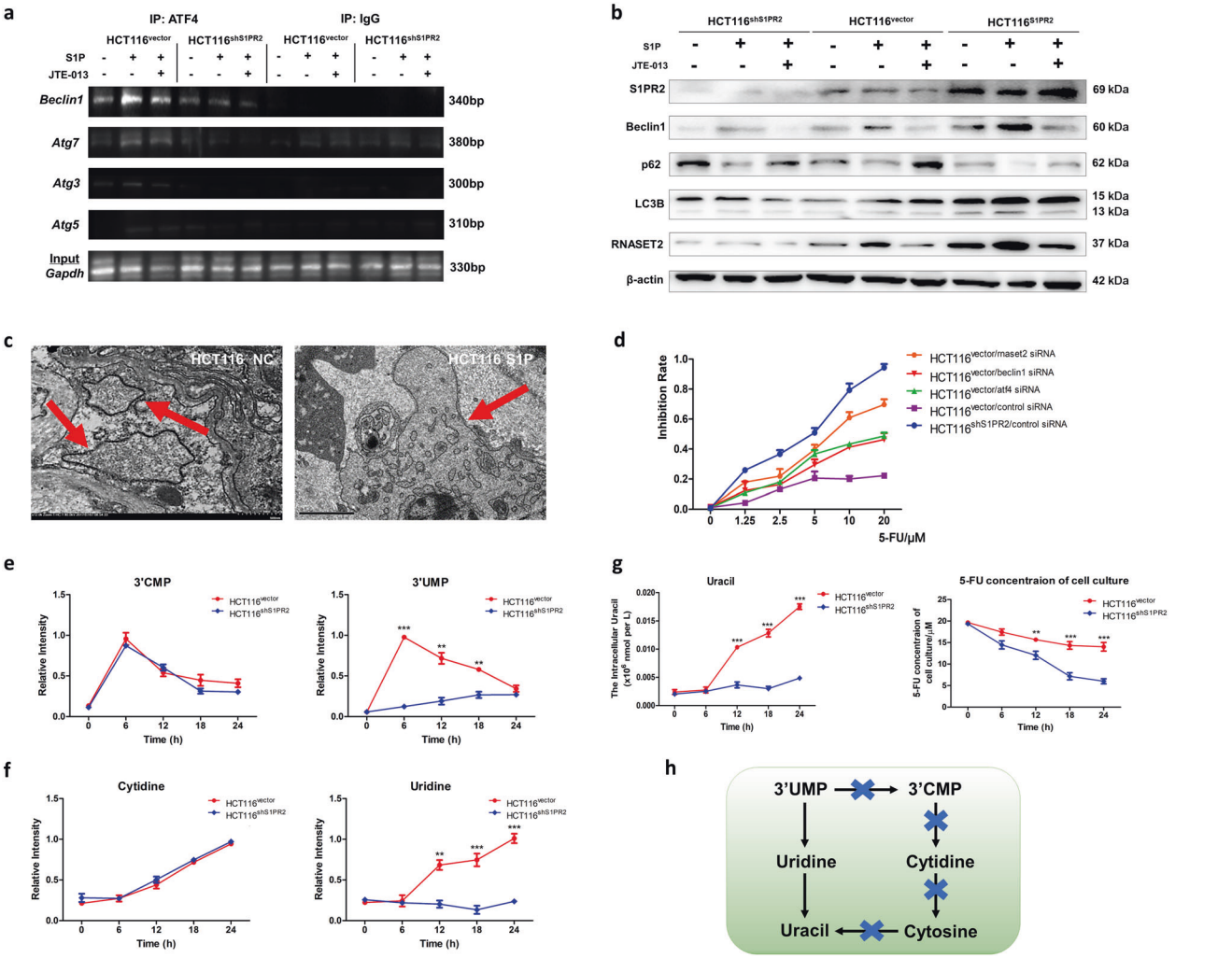

Fig. 5 Activated ATF4 upregulates RNASET2 to promote uracil generation, leading to 5-FU resistance of colorectal tumors. a ChIP assay showing the binding of ATF4 to the promoter regions of autophagy genes, *Beclin1*, *Atg7*, *Atg3*, and *Atg5*. The protein-DNA complexes were immunoprecipitated with anti-ATF4 or the negative control IgG. The sequences of the ATF4-binding regions in the autophagy gene promoters or added Gapdh DNA, taken from representative agarose gels, were amplified by semiquantitative PCR. HCT116^{vector} and HCT116^{shS1PR2} cells were exposed to S1P (10 μM), JTE-013 (10 μM), or S1P plus JTE-013 for 24 h. **b** Western blotting was used to analyze the levels of Beclin1, p62, LC3B, and RNASET2 in the HCT116^{shS1PR2}, HCT116^{vector}, and HCT116^{S1PR2} cells treated with S1P (10 μM), JTE-013 (10 μM), or S1P plus JTE-013 for 24 h. **c** Compared with the normal morphosis of intracellular lysosomes in naive HCT116 cells (left panel), TEM analysis showed typical autophagic cargos and autophagosomes in the HCT116 cells treated with S1P (10 μM) for 24 h (scale bar: 100 nm). **d** In the HCT116 cells, ATF4, Beclin1, and RNASET2 were knocked down by their respective siRNA. The inhibition rates induced by 5-FU (24 h) were detected by MTT assay. Inhibition rate $= 1 - (OD_{Drug} - OD_{Blank})/(OD_{Contro} - OD_{Blank})$, $n = 3$. **e**, **f** The levels of 3′CMP, 3′UMP, cytidine, and uridine in the HCT116^{shS1PR2} (blue) and HCT116^{vector} cells (red) were determined by UHPLC-MRM-MS assay. Cancer cells were treated with S1P (10 μM) for 6, 12, 18, and 24 h. The results are presented as normalized intensity based on peak heights of each metabolite in the HCT116^{vector} control cells ($n = 3$, two-way ANOVAs). **g** UHPLC-MRM-MS assay of intracellular uracil in the HCT116^{shS1PR2} and HCT116^{vector} cells treated with S1P (10 μM) for 6 h, 12 h, 18 h and 24 h (left panel). In addition, time-dependent 5-FU concentrations in cell cultures were also detected and are illustrated in the right panel ($n = 3$, two-way ANOVAs). **h** Schematic representation of the S1PR2 internalization-mediated uracil-related nucleotide degradation pathway. Data in (**e**–**g**) are presented as the means ± SEM. *$P < 0.05$, **$P < 0.01$, and ***$P < 0.001$ (Student's *t* test).

various Ca^{2+}-sensitive isoforms of AC [37]. In addition, cAMP also affects the elevation of Ca^{2+} at numerous levels: it directly affects cAMP effects on hyperpolarization-activated cyclic nucleotide channels and cyclic nucleotide-gated (CNG) channels [38]; indirectly affects protein kinase A (PKA) and exchange proteins directly activated by cAMP at numerous points during Ca^{2+} signaling, including $InsP_3$ receptors, with each $InsP_3R$ subtype a potential substrate for PKA [39], voltage-gated Ca^{2+} channels [40], etc. Accordingly, we hypothesized that S1PR2 internalization may prohibit AC from blocking one of the Ca^{2+} channels in the ER and thus increases the levels of $[Ca^{2+}]_{ER}$ to enhance the subsequent generation of intracellular uracil; this supposition deserves to be further studied in detail.

In our previous study, we found that inhibiting S1PR2 by JTE-013 effectively reversed 5-FU resistance of CRC cells both in vitro and in vivo [16]. However, the previous study was mainly focused on the chemical synthesis and pharmacological evaluation of S1PR2 inhibitors, not the underlying regulatory mechanisms, which remain obscure. In this study, we found that S1PR2 was internalized to the ER to promote RNASET2-mediated uracil generation, which blunted the uptake of 5-FU, an exogenous uracil. It was reported that the activation of ribonuclease RNASET2 is critical for ribosomal self-RNA degradation in autophagosomes. During autophagy, RNASET2 catalyzes the cleavage of ssRNA through a 2′,3′-cyclic phosphate intermediate, yielding mono- or oligonucleotides with a terminal 3′ phosphate group [41]. In this

study, our results showed that shS1PR2 impaired 3′UMP-uridine generation but not 3′CMP-cytidine production. Therefore, we suggest that the differential inhibition might be attributed to the histidine residues in the conserved catalytic CASI and CASII motifs in RNASET2. In human RNASET2, CASI spans residues 62–69, and the aligned CASII spans residues 110–121. Substrate binding might be involved in hydrophobic interactions and hydrogen binding involving phosphate groups. The CASII span forms a perfect *α*-helix, but the carbonyl groups of residues 116 and 117 do not make proper hydrogen bonds, and thus the phi and psi angles of His118 slightly deviate from the helical form [42, 43]. This conformation results in a distortion in the helix, possibly enabling a higher energy state and better mobility of the catalytic residues at 117 and 118. Different substrates bind CASI and CASII and lead to differences in 3′CMP and 3′UMP generation. However, this supposition needs to be validated by the induction of mutations in 62–69 and the 110–121 histidine residues.

Overall, understanding the mechanisms that contribute to chemoresistance has the potential to improve therapeutic planning decisions. Changes in drug metabolism may result in cancer cells acquiring chemoresistance. This study suggests that S1P-induced S1PR2 internalization blunts 5-FU therapy by elevating autophagy-related uracil generation. Strategies for blocking S1PR2 internalization may be effective in sensitizing 5-FU-based chemotherapies.

ACKNOWLEDGEMENTS

This work was supported by the National Natural Science Foundation of China (91629303/81673449/81872884/81973350) and the Beijing Natural Science Foundation and Scientific Research Program of Municipal Commission of Education (KZ201710025020/KZ201810025033). In addition, YHZ wants to thank, in particular, the inimitable support and care from Wen-yu Wang. Hope to spend the rest of my life with you.

AUTHOR CONTRIBUTIONS

XJQ conceived the project. YHZ performed the experiments of molecular mechanisms and conducted animal studies. SBW implemented experiments of pharmaceutical analysis. SHW provided clinical samples and pathological analysis. SXC performed statistical analysis. YHZ wrote the manuscript, which was edited by all authors.

ADDITIONAL INFORMATION

The online version of this article (https://doi.org/10.1038/s41401-020-0460-0) contains supplementary material, which is available to authorized users.

Competing interests: The authors declare no competing interests.

REFERENCES

1. Soong R, Shah N, Salto-Tellez M, Tai BC, Soo RA, Han HC, et al. Prognostic significance of thymidylate synthase, dihydropyrimidine dehydrogenase and thymidine phosphorylase protein expression in colorectal cancer patients treated with or without 5-fluorouracil-based chemotherapy. Ann Oncol. 2008;19:915–9.
2. Pare L, Marcuello E, Altes A, Del RE, Sedano L, Salazar J, et al. Pharmacogenetic prediction of clinical outcome in advanced colorectal cancer patients receiving oxaliplatin/5-fluorouracil as first-line chemotherapy. Br J Cancer. 2008;99:1050–5.
3. Longley DB, Harkin DP, Johnston PG. 5-Fluorouracil: mechanisms of action and clinical strategies. Nat Rev Cancer. 2003;3:330–8.
4. Furukawa T, Tabata S, Yamamoto M, Kawahara K, Shinsato Y, Minami K, et al. Thymidine phosphorylase in cancer aggressiveness and chemoresistance. Pharmacol Res. 2018;132:15–20.
5. Crea F, Nobili S, Paolicchi E, Perrone G, Napoli C, Landini I, et al. Epigenetics and chemoresistance in colorectal cancer: an opportunity for treatment tailoring and novel therapeutic strategies. Drug Resist Update. 2011;14:280–96.
6. Wu R, Nie Q, Tapper EE, Jerde CR, Dunlap GS, Shrestha S, et al. Histone H3K27 trimethylation modulates 5-fluorouracil resistance by inhibiting PU.1 binding to the DPYD promoter. Cancer Res. 2016;76:6362–73.
7. Marjaneh RM, Khazaei M, Ferns GA, Avan A, Aghaee-Bakhtiari SH. The role of microRNAs in 5-FU resistance of colorectal cancer: possible mechanisms. J Cell Physiol. 2019;234:2306–16.
8. Lifshitz V, Priceman SJ, Li W, Cherryholmes G, Lee H, Makovski-Silverstein A, et al. Sphingosine-1-phosphate receptor-1 promotes environment-mediated and acquired chemoresistance. Mol Cancer Ther. 2017;16:2516–27.
9. Guo YX, Ma YJ, Han L, Wang YJ, Han JA, Zhu Y. Role of sphingosine 1-phosphate in human pancreatic cancer cells proliferation and migration. Int J Clin Exp Med. 2015;8:20349–54.
10. Dempsey LA. Distinct S1PR roles. Nat Immunol. 2019;20:517.
11. Ogretmen B. Sphingolipid metabolism in cancer signalling and therapy. Nat Rev Cancer. 2018;18:33–50.
12. Aarthi JJ, Darendeliler MA, Pushparaj PN. Dissecting the role of the S1P/S1PR axis in health and disease. J Dent Res. 2011;90:841–54.
13. Stepanovska B, Huwiler A. Targeting the S1P receptor signaling pathways as a promising approach for treatment of autoimmune and inflammatory diseases. Pharmacol Res. 2020;154:104170.
14. Calebiro D, Nikolaev VO, Persani L, Lohse MJ. Signaling by internalized G-protein-coupled receptors. Trends Pharmacol Sci. 2010;31:221–8.
15. Mullershausen F, Zecri F, Cetin C, Billich A, Guerini D, Seuwen K. Persistent signaling induced by FTY720-phosphate is mediated by internalized S1P1 receptors. Nat Chem Biol. 2009;5:428–34.
16. Zhang YH, Luo DD, Wan SB, Qu XJ. S1PR2 inhibitors potently reverse 5-FU resistance by downregulating DPD expression in colorectal cancer. Pharmacol Res. 2020;155:104717.
17. Ou J, Peng Y, Yang W, Zhang Y, Hao J, Li F, et al. ABHD5 blunts the sensitivity of colorectal cancer to fluorouracil via promoting autophagic uracil yield. Nat Commun. 2019;10:1078.
18. Parang B, Barrett CW, Williams CS. AOM/DSS model of colitis-associated cancer. Methods Mol Biol. 2016;1422:297–307.
19. Hait NC, Allegood J, Maceyka M, Strub GM, Harikumar KB, Singh SK, et al. Regulation of histone acetylation in the nucleus by sphingosine-1-phosphate. Science. 2009;325:1254–7.
20. Wang H, Zhang J, Hu SH, Tan SZ, Zhang B, Zhou HM, et al. Real-time microwave exposure induces calcium efflux in primary hippocampal neurons and primary cardiomyocytes. Biomed Environ Sci. 2018;31:561–71.
21. Parang B, Barrett CW, Williams CS. AOM/DSS model of colitis-associated cancer. Methods Mol Biol. 2016;1422:297–307.
22. Kharel Y, Raje M, Gao M, Gellett AM, Tomsig JL, Lynch KR, et al. Sphingosine kinase type 2 inhibition elevates circulating sphingosine 1-phosphate. Biochem J. 2012;447:149–57.
23. Spiegel S, Milstien S. Sphingosine-1-phosphate: an enigmatic signalling lipid. Nat Rev Mol Cell Biol. 2003;4:397–407.
24. Lee DK, Min YS, Yoo SS, Shim HS, Park SY, Sohn UD. Effect of sphingosine-1-phosphate on intracellular free Ca^{2+} in cat esophageal smooth muscle cells. Biomol Ther. 2018;26:546–52.
25. Villa A, Podini P, Panzeri MC, Soling HD, Volpe P, Meldolesi J. The endoplasmic-sarcoplasmic reticulum of smooth muscle: immunocytochemistry of vas deferens fibers reveals specialized subcompartments differently equipped for the control of Ca^{2+} homeostasis. J Cell Biol. 1993;121:1041–51.
26. Auberger P, Puissant A. Autophagy, a key mechanism of oncogenesis and resistance in leukemia. Blood. 2017;129:547–52.
27. Wu HB, Yang S, Weng HY, Chen Q, Zhao XL, Fu WJ, et al. Autophagy-induced KDR/VEGFR-2 activation promotes the formation of vasculogenic mimicry by glioma stem cells. Autophagy. 2017;13:1528–42.
28. Wu QB, Sheng X, Zhang N, Yang MW, Wang F. Role of microRNAs in the resistance of colorectal cancer to chemoradiotherapy. Mol Clin Oncol. 2018;8:528–32.
29. Jeon SJ, Ahn JH, Halder D, Cho HS, Lim JH, Jun SY, et al. TIPRL potentiates survival of lung cancer by inducing autophagy through the eIF2alpha-ATF4 pathway. Cell Death Dis. 2019;10:959.
30. Thorn A, Steinfeld R, Ziegenbein M, Grapp M, Hsiao HH, Urlaub H, et al. Structure and activity of the only human RNase T2. Nucleic Acids Res. 2012;40:8733–42.
31. Haud N, Kara F, Diekmann S, Henneke M, Willer JR, Hillwig MS, et al. rnaset2 mutant zebrafish model familial cystic leukoencephalopathy and reveal a role for RNase T2 in degrading ribosomal RNA. Proc Natl Acad Sci USA. 2011;108:1099–103.
32. Antoon JW, White MD, Slaughter EM, Driver JL, Khalili HS, Elliott S, et al. Targeting NFkB mediated breast cancer chemoresistance through selective inhibition of sphingosine kinase-2. Cancer Biol Ther. 2011;11:678–89.
33. Mathes C, Fleig A, Penner R. Calcium release-activated calcium current (ICRAC) is a direct target for sphingosine. J Biol Chem. 1998;273:25020–30.
34. Meyer ZHD. Lysophospholipid receptor-dependent and -independent calcium signaling. J Cell Biochem. 2004;92:937–48.
35. Melendez AJ. Sphingosine kinase signalling in immune cells: potential as novel therapeutic targets. Biochim Biophys Acta. 2008;1784:66–75.
36. Reuschlein AK, Jakobsen E, Mertz C, Bak LK. Aspects of astrocytic cAMP signaling with an emphasis on the putative power of compartmentalized signals in health and disease. Glia. 2019;67:1625–36.

37. Halls ML, Cooper DM. Regulation by Ca2+-signaling pathways of adenylyl cyclases. Cold Spring Harb Perspect Biol. 2011;3:a4143.
38. Michalakis S, Becirovic E, Biel M. Retinal cyclic nucleotide-gated channels: from pathophysiology to therapy. Int J Mol Sci. 2018;19:749.
39. Straub SV, Wagner LN, Bruce JI, Yule DI. Modulation of cytosolic calcium signaling by protein kinase A-mediated phosphorylation of inositol 1,4,5-trisphosphate receptors. Biol Res. 2004;37:593–602.
40. Dai S, Hall DD, Hell JW. Supramolecular assemblies and localized regulation of voltage-gated ion channels. Physiol Rev. 2009;89:411–52.
41. Luhtala N, Parker R. T2 Family ribonucleases: ancient enzymes with diverse roles. Trends Biochem Sci. 2010;35:253–9.
42. Suzuki A, Yao M, Tanaka I, Numata T, Kikukawa S, Yamasaki N, et al. Crystal structures of the ribonuclease MC1 from bitter gourd seeds, complexed with 2'-UMP or 3'-UMP, reveal structural basis for uridine specificity. Biochem Biophys Res Commun. 2000;275:572–6.
43. Van Triest B, Pinedo HM, Giaccone G, Peters GJ. Downstream molecular determinants of response to 5-fluorouracil and antifolate thymidylate synthase inhibitors. Ann Oncol. 2000;11:385–91.